HHS Public Access

Author manuscript

Nat Chem. Author manuscript; available in PMC 2016 November 01.

Published in final edited form as:

Nat Chem. 2016 May ; 8(5): 476–483. doi:10.1038/nchem.2472.

Self-assembly of size-controlled liposomes on DNA nanotemplates

Yang Yang[1,2,†], **Jing Wang**[1,2,†], **Hideki Shigematsu**[3,‡], **Weiming Xu**[1,2], **William M Shih**[4,5,6,*], **James E Rothman**[1,2,*], and **Chenxiang Lin**[1,2,*]

[1]Department of Cell Biology, Yale University School of Medicine

[2]Nanobiology Institute, Yale University

[3]Department of Cellular and Molecular Physiology, Yale University School of Medicine

[4]Wyss Institute for Biologically Inspired Engineering, Harvard University

[5]Department of Biological Chemistry and Molecular Pharmacology, Harvard Medical School

[6]Department of Cancer Biology, Dana-Farber Cancer Institute

Abstract

Artificial lipid-bilayer membranes are valuable tools for the study of membrane structure and dynamics. For applications such as studying vesicular transport and drug delivery, there is a pressing need for artificial vesicles with controlled size. However, controlling vesicle size and shape with nanometer precision is challenging and approaches to achieve this can be heavily affected by lipid composition. Here we present a bio-inspired templating method to generate highly monodispersed sub-100nm unilamellar vesicles, where liposome self-assembly was nucleated and confined inside rigid DNA nanotemplates. Using this method we produced homogenous liposomes with four distinct pre-defined sizes. We also show that the method can be used with a variety of lipid compositions and probed the mechanism of the templated liposome formation by capturing key intermediates during membrane self-assembly. The DNA nanotemplating strategy represents a conceptually novel way to guide the lipid bilayer formation, and could be generalized to engineer complex membrane/protein structures with nanoscale precision.

*Correspondence to: chenxiang.lin@yale.edu (C.L.), james.rothman@yale.edu (J.E.R.) and william_shih@dfci.harvard.edu (W.M.S.).
†These authors contributed equally.
‡Current address: Division of Structural and Synthetic Biology, RIKEN Center for Life Science Technologies
Correspondence and requests for materials should be addressed to C.L., J.E.R. and W.M.S.

Author contributions:

Y.Y. and J.W. designed and conducted the majority of the experiments, analyzed the data, prepared the majority of the manuscript and contributed equally to this work. H.S. performed cryo-EM study and prepared the manuscript. W.X. initiated the project, developed DNA-lipid conjugation method, and designed and performed pilot experiments to prepare and purify DNA-ring enclosed vesicles. W.M.S. initiated the project and discussed the results. J.E.R. initiated the project, supervised J.W. and W.X., and discussed the results. C.L. initiated the project, designed and supervised the study, interpreted the data and prepared the manuscript. All authors reviewed and approved the manuscript.

Competing financial interests:

Authors declare no competing financial interests.

Introduction

Cell membranes are tremendously complex in structure and function. They define cellular compartments and mediate biomolecule transport. A central task of cell biology is to elucidate the interplays between lipid bilayers and other molecules (e.g. protein) that drive membrane dynamics and govern cell behaviors[1]. Using an artificial membrane with well-defined properties is a powerful approach to analyze sophisticated cellular machinery in a controlled system with reduced complexity[2]. Engineering a customized lipid bilayer membrane is also an intriguing goal in biotechnology, which can open up opportunities such as drug delivery and biosensing[3–5].

An abundance of methods have been developed to create artificial membranes, especially in the form of unilamellar vesicles[6,7]. Manufacturing lipid vesicles generally include the following three steps: first, lipids are dissolved in a good solvent (e.g. oil, chloroform, aqueous solution with detergent) where they are dispersed as single molecules or small aggregates (e.g. micelles); second, lipids are transferred into detergent-free aqueous solution to allow the self-assembly of bilayer membranes that eventually form vesicles. This can be achieved in a number of ways including drying/rehydration, dialysis and reverse phase evaporation[8–11]. Tuning the experimental conditions at this stage is often effective to generate vesicles with desired properties[12–16]. Third, an external force (e.g. sonication, extrusion) can be applied to the vesicles to control their size and improve the monodispersity[17–20]. Despite the breakthroughs for producing vesicles of controlled geometry and surface chemistry, existing techniques have one or more of the following limitations: (i) it still remains challenging to control the vesicle size (let alone the shape) with nanometer precision. (ii) the experimental conditions required for a specific vesicle type are often empirically determined and may suffer from batch-to-batch difference. (iii) some size-control methods depend heavily on lipid composition, which limits their adaptability[12]. (iv) certain techniques entail the use of specialized experimental apparatus that are not readily available to a common biochemistry lab[21–23].

Inspired by the protein machineries that sculpt and scaffold the membrane structures in cells[24], a reasonable hypothesis is that high-precision membrane engineering can be achieved *in vitro* through a similar templating approach[25]. Previously, DNA has been proven as a nanoscale material capable of gluing and fusing pre-assembled liposomes[26–28]. To generate the programmable nanotemplates for vesicles, we took advantage of an emerging technique termed “structural DNA nanotechnology”[29,30]. Through the rational design of DNA-strand hybridization, this technique generates self-assembled nanostructures with programmable geometry, addressable surface and outstanding structural stability. More specifically, we utilized the “DNA-origami”[31,32] technique to fold a single-stranded DNA (scaffold strand) into customized shape with the help of many DNA oligonucleotides (staple strands). We then decorated the interior surface of the DNA-origami nanostructures with lipid molecules and used them to guide the formation of liposomes. In this way, we were able to obtain a series of highly monodispersed liposomes with sizes designed to be 29, 46, 60 and 94 nm. The methods also worked nicely on a variety of lipid compositions. Although others have successfully produced vesicles with artificial templates surrounded by membranes (i.e. endoskeleton)[33–35], our method differs in that the DNA-nanostructure

worked as the “exoskeleton” and lead to vesicles with controlled size in a wider range and potentially with more versatile functions. Furthermore, this system provides a unique tool for studying nucleated lipid assembly into a liposome within a rigid template. We studied the mechanism of such templated vesicle formation by capturing critical intermediates during the bilayer self-assembly.

Results

We designed four different DNA-origami rings (Supplementary Figure S1) and used them as templates to define the liposome size. The scheme of the DNA-ring templated liposome production is depicted in Figure 1. Taking the 12-helix-bundle ring with 60-nm inner diameter for example, the DNA ring was assembled by mixing an 8064-nt scaffold strand and 225 staple strands in the molar ratio of 1:6 followed by 36 hours of thermal annealing and purified by rate-zonal centrifugation[36] (Supplementary Figure S2). A well-folded ring carried sixteen 21-nt single-stranded DNA handles spaced evenly along an inner DNA helix and pointed toward the center of the ring. It also carried eight evenly spaced outer-handles (not shown in Figure 1 for clarity, for more details see Supplementary Figure S3). The inner- and outer-handles were designed to have orthogonal sequences. A thiol-modified DNA strand complementary to the inner-handle (anti-inner-handle) was chemically conjugated with 1,2-dioleoyl-sn-glycero-3-phosphoethanolamine-N-[4-(p-maleimidophenyl)butyramide] (18:1 MPB PE) *via* thiol-maleimide cross-linking reaction. To label the DNA rings with fluorescently modified anti-outer-handles and lipidated anti-inner-handles, rings were mixed with an excessive amount of anti-handles in a solution containing 1% *n*-Octyl-beta-D-Glucopyranoside (OG) to allow for hybridization. The fluorescently labeled DNA ring-lipid complex was subsequently mixed with extruded liposomes (~1:188,000 ring:lipid molar ratio) in a solution containing OG at its critical micelle formation concentration (CMC) of 0.67% (w/v). The solution was then dialyzed for 16 hours to allow for detergent removal and liposome formation. Finally, the detergent-free solution was loaded to an iodixanol gradient and spun in an ultracentrifuge to separate the crude products based on their buoyant density.

The first method we used to characterize our product is gel electrophoresis. As shown in Figure 2a, fractions collected after isopycnic centrifugation were resolved on an agarose gel with 0.05% Sodium dodecyl sulfate (SDS), which served to disrupt membranes into lipid-detergent micelles. Because DNA rings and membranes were labeled with Cyanine-5 (Cy5) modified anti-outer-handle and Rhodamine(B)-PE (Rhod-PE), respectively, they fluoresced in two separate channels (pseudo-colored green and red). The first fraction (least dense, F1) contained only free lipid aggregates, without any DNA rings. In the second through seventh fractions (F2–F7), DNA rings coexisted with lipids, suggesting the formation of DNA-ring associated vesicles. The denser fractions (F8–F12) contained neither DNA nor lipid. In contrast, in the absence of inner-handle and/or lipid modified anti-inner-handle (Supplementary Figure S4), F8–F12 contained only DNA rings while F1–F7 contained only lipids. Therefore, the association between DNA ring and lipid in the final product depends critically on the presence of the lipid molecules initially attached to the inside of the DNA ring.

Then we used transmission electron microscopy (TEM) to examine each fraction. A set of representative images are shown in Figure 2a (more images can be found in Supplementary Figure S5–S6). Under the negative-stain condition, vesicles occupied larger volumes than the DNA-origami rings under the uranium stain layer, thus appearing lighter in the grayscale images. Fraction 3 and 4 contained mostly “templated vesicle” structures where each DNA ring appeared to be completely filled with a liposome. Together, these two fractions contained nearly half (~ 58%) of the DNA rings, meaning that such templated vesicles were the main product. The byproducts included DNA rings attached to bigger and/or multiple liposomes found in F2, and rings with smaller liposomes found in F5–F7. The size distribution of liposomes from F2 to F7 is shown in Supplementary Figure S6. It is worth noting that the appearance of the vesicles varied considerably across different areas on the TEM grid, ranging from a uniformly white circle to a cup-like shape (edges brighter than the center). This is likely due to the unevenness of the stain and vesicle dehydration during TEM sample preparation; both are common effects known to associate with the negative-stain TEM techniques[35,37].

Using cryo-electron microscopy (cryo-EM), we confirmed that the templated liposomes were spherical and unilamellar. On the cryo-specimen grid, a thin layer of sample was rapidly frozen in amorphous ice (~110–140 nm in thickness), which preserved the nanostructures in 3D space without staining or fixing[38,39]. Thus, the DNA ring templated liposomes were observed in their hydrated state through various EM projections. To enhance contrast, cryo-EM images were taken with two defocuses and merged by a computer program[40]. As shown in Figure 2b, the membranes appeared as dark annuli with widths of 5.28 nm ± 0.54 nm regardless of the EM projection, proving that the liposomes were spherical and unilamellar. On the other hand, the DNA rings surrounding the liposomes appeared as light gray tracks with different shapes (e.g. line, ellipse and circle) depending on the EM projection angles, consistent with our design. In many cases, the DNA ring appeared to occupy the equatorial plane of the liposome, much like Saturn. The vesicle size was measured to be 50.0± 4.6 nm (Supplementary Figure S7) using cryo-EM, which was ~8 nm smaller than that measured by negative-stain TEM (58.1±8.3 nm). This small discrepancy can be attributed to the vesicle dehydration and deformation during the negative stain process.

We applied similar protocols for sample preparation, purification and characterization to the other three DNA rings with inner diameters of 29, 46 and 94 nm. Gel electrophoresis (Supplementary Figure S5) and TEM analyses (Figure 2c & Supplementary Figure S8) confirmed that the main product in each case was the templated liposome with its diameter closely matching the inner diameter of the DNA ring (22.1±2.5 nm, 45.5±4.4 nm and 94.6±7.4 nm). We further confirmed the homogeneity of the templated vesicles by fitting their measured diameter histograms with Gaussian distribution curves (Figure 2d). In each case, at least 85% of the liposomes were within a homogenous population with the expected size, while a minor population (<15%) appeared to be smaller in diameter, possibly due to the contamination during fractionation. Compared to liposomes generated by the traditional extrusion method (Supplementary Figure S9), these DNA-nanostructure templated liposomes feature size predictability (liposome diameter matches better with the design) and superior monodispersity (a more homogenous population with smaller standard deviation).

See Technical Notes in SI for a comparison of monodispersity with other established methods.

To test the versatility of our method, we made liposomes using the same 60-nm ring as template but with different lipid compositions. As shown in Table 1, the cylindrical and electrically neutral lipid DOPC was used as the main lipid source for most conditions. Results presented in Figure 2 were produced using ~80% DOPC, 5% PEG-2k-PE and 15% DOPS (composition 0). With lipid to DNA ring ratio remaining the same, replacing PEG-2k-PE with DOPC (composition 1) resulted in main products with slightly smaller buoyant density, as characterized by isopycnic centrifugation. Using nearly 100% DOPC (composition 2) resulted in products with almost the same buoyant density as those made from composition 1. Further, with ~90% DOPC and 10% positively charged DOTAP (composition 3), products were shifted to even lighter fractions in the density gradient (Supplementary Figure S10). TEM analyses revealed these products with smaller buoyant density as DNA-membrane complexes with liposomes larger than the DNA rings. Therefore, lipid composition significantly affected the yield of the templated liposomes. In particular, a lipid with bulky (e.g. PEG-2k-PE) or negatively charged (e.g. phosphatidylserine) head groups appeared to limit the overgrowth of the liposome, while a positively charged lipid (e.g. DOTAP) did the opposite. However, the yield of templated liposomes can be rescued for lipid composition 1, 2 and 3 when the lipid to DNA ring ratio was reduced to half (i.e. ~94,000:1, Supplementary Figure S10). Thus the lipid concentration may also affect the liposome formation kinetics and outcome. In addition, we replaced DOPC in composition 0 with high-transition temperature lipid DPPC and cholesterol, and were able to generate templated liposomes with a comparable yield (composition 4 in Table 1, Supplementary Figure S10). Thus the DNA-templated vesicle assembly approach is deemed effective in producing size-controlled liposomes across a range of lipid compositions.

We further demonstrated that the DNA ring can be enzymatically removed from the templated liposome with minimal effect on the liposome size. As shown in Figure S11, the liposomes formed inside the 60-nm rings remained largely unchanged (63.0±9.1 nm *vs* 58.1±8.3 nm) after ring removal by DNaseI. The slight (~8%) increase in observed diameter can be attributed to a more severe liposome deformation without the DNA template during TEM sample preparation. While liposomes made of composition 0 (containing 5% PEG-2k-PE) maintained their homogeneity for 2 weeks with or without DNA template, liposomes made of composition 1 (containing no PEG-2k-PE) aggregated and fused within 4 hours after the template removal (Supplementary Figure S11). Therefore, the liposome stability appeared to be governed by the steric protection (repulsion) posed by PEG-2k-PE and the van der Waals attraction between zwitterionic DOPC molecules. Such vesicle stability dependency on lipid composition is consistent with previous reports[41–43].

After producing monodispersed liposomes with pre-defined sizes, we studied the DNA-ring templated liposome formation mechanism using two approaches. First, the stoichiometry and spatial positioning of the anti-handle modified lipid molecules relative to the DNA ring were systematically varied and the subsequent changes in the liposome formation were characterized. Second, the dialysis process was stopped at various time points to capture critical intermediates during membrane self-assembly.

The modularity and addressability of the DNA-origami structure allowed us to readily change the number and position of the DNA handles (and hence the anti-handle modified lipid). For instance, variants of the 60-nm ring can be designed to carry 0–16 inner handles for lipid attachment. As described above, rings without inner handles resulted in no association between the ring and vesicle. Further, the vesicle formation results were compared among rings bearing 2, 4, 8 and 16 pre-attached lipid molecules (lipid seeds) inside. After isopycnic centrifugation, the quantities of the DNA rings in fraction 1–7 were plotted in Figure 3a. It is obvious that the yield of a ring with a liposome of desired size (F3 & F4) positively correlates with the number of lipid seeds inside the ring. For example, a ring with 2 lipid seeds gave merely 23% yield of desired product, a dramatic decrease from the 58% yield achieved by the ring with 16 seeds. Variants with different inner handles were designed based on the 46-nm ring and the same trend was confirmed (Supplementary Figure S12). Next, the position of the lipid seed was changed from the distal end to the proximal end of the handle/anti-handle duplex to bring the seeds closer to the 29-nm DNA ring. This change shifted the mean diameter of liposomes in F5 (the fraction containing the most DNA rings, Supplementary Figure S13) from 14 nm to 22 nm, matching well with the cartoon models shown in Figure 3b, where the lipid modified duplexes were considered as rigid rods. The lipid seed position was further changed from the inside to the outside of the ring. This was achieved by placing the handles on different DNA double helices of the ring (Figure 3c). Four variants of the 46-nm ring were constructed for this purpose, each carrying 3 handles forming 0°, 60°, 120° or 180° angles with the ring. With the lipid seeds inside (handles at 0° and 60°), most of the rings had liposomes formed within their boundaries, promoting the formation of templated liposomes. In contrast, with handles flipped (180° and 120°), most rings had liposomes formed outside, causing the formation of aggregates. To illustrate this difference, the number of liposomes associated with a ring in one of the density gradient fractions (F4) is plotted in Figure 3c (more images in Supplementary Figure S14). It is obvious that the rings with lipid seeds inside favored the formation of a single liposome per ring while those with lipid seeds outside yielded a significant amount of three well-separated liposomes surrounding a ring. These findings lead us to the hypothesis that the self-assembly of templated vesicles is initially nucleated by the lipid seeds and is finally restricted by the rigid body of the DNA-origami ring.

To test our hypothesis, we performed a second set of experiments to capture the intermediate structures during the liposome formation. Based on previous mechanistic studies of vesicle reconstitution from lipid-detergent micelles[44–48], we reasoned that the formation of the templated vesicles completes during the dialysis of OG. To determine the important time points of dialysis, radioactive OG was used to track the amount of detergent remaining at 0, 0.5, 1, 3, 3.5, 5, and 16 hour. As shown in Figure 4a, the detergent concentration change followed a single exponential curve. After 1 hour of dialysis, the OG in the lipid-detergent mixture was diluted to 0.093%, equivalent to ~20% of the CMC; After 3 hours, the OG level dropped to background. Therefore, we imaged samples after 0, 0.5, 1, 1.5, and 16-hour dialysis and further categorized the DNA rings based on their lipid/detergent association states. For the purpose of this study, only the rings with clear boundaries were included for statistics (e.g. rings covered by a larger lipid/detergent aggregates were not counted in).

We performed such mechanistic study on 60-nm rings, and again systematically varied the number of lipid seeds inside of each ring (0, 4, 8 and 16). As expected, DNA-rings without lipid seeds remained empty throughout the dialysis (data not shown). For the ring initially modified with 4 lipid molecules, the observations (Figure 4b) are as follows. Without dialysis (0.67% OG), rings lacked noticeable lipid attachment. After 30-min of dialysis (0.23% OG), in addition to such empty DNA structures, rings appeared to be decorated with a substantial amount of lipid. The DNA-lipid association at this stage mainly took two forms: most of the DNA rings bare a strip of worm like lipid-detergent micelle (mean thickness = 5.2 nm) on the inside, while some of the DNA rings appeared to be wrapped tightly by a continuous lipid bilayer (see Supplementary Figure S15 for more images). At 1 hour (0.093% OG), the population of empty rings further decreased and more rings appeared to be associated with worm like micelles or wrapped by a continuous bilayer. After 1.5 hour dialysis (0.037% OG), aside from these intermediates, about one third of the DNA rings started to attach with one to four separated vesicles (mean diameter = 18 nm) on the inside. A small population of rings each fully filled with a liposome (Saturn-like structures) also emerged. Finally, with detergent completely removed after overnight dialysis, the majority of the rings were either fully filled with a single liposome or associated with a few separate vesicles, while a minority of rings remained empty. Other structures found at 0.5, 1 and 1.5 hour were almost completely absent from the detergent-free mixture. When the number of lipid seeds per ring was changed to 8 and 16, similar observations were made with two exceptions after 1.5 hours of dialysis. First, in addition to associating with individual small liposomes, rings modified with 8 or 16 lipid seeds encompassed a toroidal membrane structure with a mean section diameter of 15 nm. Second, compared with rings having 4 lipid seeds, more rings were fully filled after 1 hour of dialysis. This difference became more obvious after 1.5 hours and eventually resulted in a higher percentage of size-controlled liposomes in the final detergent-free mixture, which is consistent with our findings shown in Figure 3a.

Although extreme care has to be taken when interpreting the negative-stain TEM data, the following trends are obvious from the mechanistic study. First, the association between the DNA ring and lipid bilayer depends on the presence of lipid seeds, confirming their role as nucleation points. Second, the total mass of lipid associated with a ring increases continuously as the detergent concentration decreases, suggesting a gradual growth process as opposed to the direct capture of a liposome. Third, the formation of size-controlled liposomes (Saturn-like structures) accelerates when more lipid molecules were initially placed on the ring, suggesting that faster bilayer growth and merger can be driven by a higher number of nucleation sites packed in a confined space. These findings strongly supported our hypothesis of templated liposome formation (Figure 4c): The lipid seeds inside the DNA ring were initially stabilized by small clusters of lipid-detergent micelle (Figure 4c, top row); As the detergent concentration decreases, they merge and expand in 1-D to form worm like micelles, which further expand in 2-D and curve up (in 3-D) to form lipid-bilayer structures resembling a doughnut (Figure 4c, middle row); Such intermediates become unstable when detergent is further diluted and eventually lead to the formation of liposomes inside the ring (Figure 4c, bottom row). The Saturn-like structures are favored when a high density of seeds are present within a rigid DNA frame.

Discussion

In summary, we have presented a strategy to generate small unilamellar vesicles (SUV) through nano-templating. The programmable vesicle size, outstanding vesicle mono-dispersity and versatility to produce SUVs with different lipid compositions are the most valuable features of this system. In addition, the liposomes self-assemble during a simple detergent removal process (e.g. dialysis as demonstrated here, or direct dilution/adsorption as explored by others[46,48]), making this method easily accessible to the general research community, and more importantly, compatible for loading cargos such as nucleic acids, antibody, and small molecules[4]. Other natural and synthetic amphipathic molecules could in principle be incorporated to functionalize and varietize the vesicles. The virtually complete OG depletion and the decent vesicle stability (lipid composition 0) are promising features that point to an outstanding membrane integrity[5,46]. However, unlike a template-free vesicle formation process, here the DNA nanotemplate dictates the outcome of membrane self-assembly by providing a nucleation site to start lipid aggregation, a rigid structure to confine the vesicle growth, and an added mass to facilitate purification. In this work we focused on producing sub-100 nm vesicles at an analytical scale (up to ~100 μL of 0.9 mM lipid) to prove the concept. However, with the availability of 3D DNA nanostructures larger than 100 nm[49,50], it is conceivable that this nano-templating technique could be generalized to make large unilamellar vesicles with similar features. We note that this technique requires much improvement in cost efficiency, lipid recovery rate, and scalability to meet the needs of many biomedical applications (see Technical Notes in SI for further discussion). However, the method in its current form serves adequately to probe the mechanism of nucleated liposome growth and holds great promise in studying protein behaviors on membranes with defined curvatures.

In biological cells, membranes appear in different shapes and constantly change their chemical and physical properties to accommodate the cell's needs to grow, divide, communicate, and maintain homeostasis. Now that we have established a method to guide membrane formation *in vitro* by DNA nanotemplates, we aspire to better understand and mimic such elegance of nature in our future studies. For example, membrane deforming proteins (e.g. SNARE, BAR-domain proteins) could be organized on the DNA template to mediate membrane remodeling and rigorously study protein-membrane interactions. Also, vesicles with non-spherical (e.g. tubular) shapes could be constructed using designer DNA templates. Moreover, reconfigurable DNA structures may be built to deform the membrane in a step-wise, controlled manner. Finally, more advanced membrane manipulation techniques based on a similar concept could open up new opportunities in biotechnology such as targeted drug delivery across a membrane barrier and programmable neuron communication.

Methods Summary

Preparation of lipidated DNA anti-handles

Thiol-modified DNA oligonucleotides (Integrated DNA Technologies) were treated with *tris*(2-carboxyethyl)phosphine (Sigma-Aldrich) for 30 minutes (20 nmole DNA per reaction) and immediately reacted with 0.4 μmole of 18:1 MPB PE (Avanti Polar Lipids) in aqueous

solutions containing ~2% OG (EMD Millipore) at room temperature for 45 minutes. Such a reaction mixture was then diluted 2-fold, added to 0.6 μmole of pre-dried lipids, agitated and dialyzed overnight in order to incorporate lipidated DNA molecules into liposomes. The conjugation products were separated from unconjugated DNA *via* isopycnic centrifugation in iodixanol gradients (Cosmo Bio USA) and later analyzed by SDS-polyacrylamide gel electrophoresis.

DNA-origami ring design and preparation

The DNA-origami rings were designed using caDNAno (caDNAno.org). Inner and outer-handle sequences (21-nt) were generated by NUPACK (nupack.org) and manually added to the 3′-ends of the appropriate staple strands. DNA scaffold strands (3024-, 7308-, 7560-, or 8064-nt) were produced using *E.coli* and M13-derived bacteriophages. Staple strands were synthesized by Integrated DNA Technologies. The DNA rings were assembled from a scaffold strand (50 nM) and a pool of staple strands (300 nM each) in 5mM Tris•HCl, 1 mM EDTA, pH 8.0 with 10 or 12 mM of $MgCl_2$ using a 36-hour thermal annealing program. Correctly assembled DNA nanostructures were purified *via* rate-zonal centrifugation in glycerol gradients as described previously[36].

Preparation of DNA-ring templated liposomes

DNA rings were first labeled with lipidated anti-inner-handles and Cy5-modified anti-outer-handles in one-pot hybridization mixtures containing 1% OG. To form DNA-ring templated liposomes, 15 μL of 1× hydration buffer (25 mM HEPES, 400 mM KCl, 10 mM $MgCl_2$, pH 7.5) and 5 μL of 15 mM rehydrated lipid mixture (compositions shown in Table 1) were added to 40 μL of 10 nM lipid- & Cy5- labeled DNA ring. The solution was gently shaken for 30 minutes at room temperature, diluted with 60 μL of 1× hydration buffer containing 0.67% OG, put into a 7kD molecular weight cut-off dialysis cassette (Thermo Scientific), and dialyzed against 2 L of 1× hydration buffer for 16 hours. The dialyzed solutions were subjected to isopycnic centrifugation in iodixanol gradients. Recovered fractions were analyzed by SDS-agarose gel electrophoresis to determine to their contents. Optionally, DNase I (Thermo Scientific) was used to remove DNA rings per manufacturer's recommendation.

Electron Microscopy

Negative-staining was achieved by adsorbing ~5 μL of sample on a glow-discharged formvar/carbon coated copper grid (Electron Microscopy Sciences) and staining with 2% uranyl formate. Imaging was performed on a JEOL JEM-1400 Plus microscope operated at 80kV. Samples for cryo-EM were first concentrated using centrifugal filters with 30-kD nominal molecular weight limit (EMD Millipore) to remove iodixanol and achieve ~50 nM DNA-ring concentration. The concentrated samples were then adsorbed on glow-discharged holey carbon grids (Quantifoil MicroTools GmbH), which were subsequently washed with buffer solution with 10% reduced salt concentration, blotted, and flash frozen in liquid ethane using FEI Vitrobot. Imaging was performed on an FEI Tecnai-F20 microscope operated at 200kV.

Time-course study of liposome formation

To determine the remaining OG concentration at various time points during dialysis, 1.8 μL of ~0.01% ^{14}C-labeled OG (American Radiolabeled Chemicals) were added to a 360 μL solution containing ~6.7 nM lipid-labeled DNA ring, ~2.5 mM extra lipid and 0.67% non-radioactive OG. After 1-hour agitation, 10 μL of the mixture was set aside; the rest was diluted to ~760 μL in 1× hydration buffer with 0.67% non-radioactive OG and split into six cassettes for dialysis against 1× hydration buffer. Using a scintillation counter (Beckmann-Coulter), the radioactivity of the mixture after 0-, 0.5-, 1-, 3-, 3.5-, 5- or 16-hour dialysis was measured. The remaining OG concentrations were then calculated based on those measurements. In order to capture intermediates during detergent removal, a similar liposome formation protocol was used with non-radioactive OG and the dialysis was stopped after 0, 0.5, 1, 1.5 or 16 hours. Such dialyzed solutions were fractionated after isopycnic centrifugation and characterized by SDS-agarose gel electrophoresis and negative-stain TEM. Gel and TEM images were analyzed manually using ImageJ (National Institute of Health).

Supplementary Material

Refer to Web version on PubMed Central for supplementary material.

Acknowledgments

We thank P.D. Ellis for designing the DNA rings used for placing lipid seeds at different angles, and for proofreading the manuscript. We thank F. Sigworth for providing cryo-electron micrographs of extruded liposomes. This work is supported by a National Institutes of Health (NIH) Director's New Innovator Award (DP2-GM114830), an NIH grant (R21-GM109466) and a Yale University faculty startup fund to C.L., an NIH grant to J.E.R. (R01-DK027044), and an NIH Director's New Innovator Award (DP2-OD004641), an Army Research Office MURI grant (W911NF-12-1-0420), National Science Foundation Expeditions Grant (1317694), and a Wyss Institute for Biologically Inspired Engineering Faculty Award to W.M.S.

References

1. Cho W, Stahelin RV. Membrane-protein interactions in cell signaling and membrane trafficking. Annu Rev Biophys Biomol Struct. 2005; 34:119–151. [PubMed: 15869386]
2. Rigaud JL, Lévy D. Reconstitution of Membrane Proteins into Liposomes. Methods Enzymol. 2003; 372:65–86. [PubMed: 14610807]
3. Bally M, et al. Liposome and lipid bilayer arrays towards biosensing applications. Small. 2010; 6:2481–2497. [PubMed: 20925039]
4. Allen TM, Cullis PR. Liposomal drug delivery systems: from concept to clinical applications. Adv Drug Deliv Rev. 2013; 65:36–48. [PubMed: 23036225]
5. Çağdaş, M.; Sezer, AD.; Bucak, S. Liposomes as Potential Drug Carrier Systems for Drug Delivery. INTECH; 2014.
6. Dua J, Rana A, Bhandari A. Liposome: methods of preparation and applications. Int J Pharm Stud Res. 2012; 3:14–20.
7. Gregory, G. Liposome technology. Vol. 1. CRC press; 2006.
8. Batzri S, Korn ED. Single Bilayer Liposomes Prepared without Sonication. Biochim Biophys Acta. 1973; 298:1015–1019. [PubMed: 4738145]
9. Bosworth ME, Hunt CA, Pratt D. Liposome dialysis for improved size distributions. J Pharm Sci. 1982; 71:806–812. [PubMed: 7120068]

10. Mayer LD, Hope MJ, Cullis PR, Janoff AS. Solute Distributions and Trapping Efficiencies Observed in Freeze-Thawed Multilamellar Vesicles. Biochim Biophys Acta. 1985; 817:193–196. [PubMed: 4005257]
11. Pidgeon C, McNeely S, Schmidt T, Johnson JE. Multilayered vesicles prepared by reverse-phase evaporation: liposome structure and optimum solute entrapment. Biochemistry. 1987; 26:17–29. [PubMed: 3828297]
12. Genc R, Ortiz M, O'Sullivan CK. Curvature-tuned preparation of nanoliposomes. Langmuir. 2009; 25:12604–12613. [PubMed: 19856992]
13. Mouritsen OG. Lipids, curvature, and nano-medicine. Eur J Lipid Sci Technol. 2011; 113:1174–1187. [PubMed: 22164124]
14. Sun J, et al. Tunable rigidity of (polymeric core)-(lipid shell) nanoparticles for regulated cellular uptake. Adv Mater. 2015; 27:1402–1407. [PubMed: 25529120]
15. Schubert R. Liposome preparation by detergent removal. Methods Enzymol. 2003; 367:46–70. [PubMed: 14611058]
16. Holzer M, Barnert S, Momm J, Schubert R. Preparative size exclusion chromatography combined with detergent removal as a versatile tool to prepare unilamellar and spherical liposomes of highly uniform size distribution. J Chromatogr A. 2009; 1216:5838–5848. [PubMed: 19545872]
17. Huang C. Studies on phosphatidylcholine vesicles. Formation and physical characteristics. Biochemistry. 1969; 8:344–352. [PubMed: 5777332]
18. Olson F, Hunt CA, Szoka FC, Vail WJ, Papahadjopoulos D. Preparation of Liposomes of Defined Size Distribution by Extrusion through Polycarbonate Membranes. Biochim Biophys Acta. 1979; 557:9–23. [PubMed: 95096]
19. Hope MJ, Bally MB, Webb G, Cullis PR. Production of large unilamellar vesicles by a rapid extrusion procedure: characterization of size distribution, trapped volume and ability to maintain a membrane potential. Biochim Biophys Acta. 1985; 812:55–65. [PubMed: 23008845]
20. Silva R, Ferreira H, Little C, Cavaco-Paulo A. Effect of ultrasound parameters for unilamellar liposome preparation. Ultrason Sonochem. 2010; 17:628–632. [PubMed: 19914854]
21. Wang T, Wang N, Wang T, Sun W, Li T. Preparation of submicron liposomes exhibiting efficient entrapment of drugs by freeze-drying water-in-oil emulsions. Chem Phys Lipids. 2011; 164:151–157. [PubMed: 21185814]
22. Yu DG, et al. Self-assembled liposomes from amphiphilic electrospun nanofibers. Soft Matter. 2011; 7:8239–8247.
23. Jahn A, Lucas F, Wepf RA, Dittrich PS. Freezing Continuous-Flow Self-Assembly in a Microfluidic Device: Toward Imaging of Liposome Formation. Langmuir. 2013; 29:1717–1723. [PubMed: 23289615]
24. McMahon HT, Gallop JL. Membrane curvature and mechanisms of dynamic cell membrane remodelling. Nature. 2005; 438:590–596. [PubMed: 16319878]
25. Langecker M, Arnaut V, List J, Simmel FC. DNA nanostructures interacting with lipid bilayer membranes. Acc Chem Res. 2014; 47:1807–1815. [PubMed: 24828105]
26. Beales PA, Vanderlick TK. Specific binding of different vesicle populations by the hybridization of membrane-anchored DNA. J Phys Chem A. 2007; 111:12372–12380. [PubMed: 17997531]
27. Chan YH, van Lengerich B, Boxer SG. Effects of linker sequences on vesicle fusion mediated by lipid-anchored DNA oligonucleotides. Proc Natl Acad Sci U S A. 2009; 106:979–984. [PubMed: 19164559]
28. Dave N, Liu J. Programmable assembly of DNA-functionalized liposomes by DNA. ACS Nano. 2011; 5:1304–1312. [PubMed: 21230009]
29. Pinheiro AV, Han D, Shih WM, Yan H. Challenges and opportunities for structural DNA nanotechnology. Nat Nanotechnol. 2011; 6:763–772. [PubMed: 22056726]
30. Jones MR, Seeman NC, Mirkin CA. Nanomaterials. Programmable materials and the nature of the DNA bond. Science. 2015; 347:1260901. [PubMed: 25700524]
31. Rothemund PW. Folding DNA to create nanoscale shapes and patterns. Nature. 2006; 440:297–302. [PubMed: 16541064]

32. Dietz H, Douglas SM, Shih WM. Folding DNA into twisted and curved nanoscale shapes. Science. 2009; 325:725–730. [PubMed: 19661424]
33. Li P, et al. A pH-sensitive multifunctional gene carrier assembled via layer-by-layer technique for efficient gene delivery. Int J Nanomedicine. 2012; 7:925–939. [PubMed: 22393290]
34. Dong Y, et al. Frame-guided assembly of vesicles with programmed geometry and dimensions. Angew Chem Int Ed Engl. 2014; 53:2607–2610. [PubMed: 24488696]
35. Perrault SD, Shih WM. Virus-inspired membrane encapsulation of DNA nanostructures to achieve in vivo stability. ACS Nano. 2014; 8:5132–5140. [PubMed: 24694301]
36. Lin C, Perrault SD, Kwak M, Graf F, Shih WM. Purification of DNA-origami nanostructures by rate-zonal centrifugation. Nucleic Acids Res. 2013; 41:e40. [PubMed: 23155067]
37. Kourembanas S. Exosomes: vehicles of intercellular signaling, biomarkers, and vectors of cell therapy. Annu Rev Physiol. 2015; 77:13–27. [PubMed: 25293529]
38. Vinson PK, Talmon Y, Walter A. Vesicle-Micelle Transition of Phosphatidylcholine and Octyl Glucoside Elucidated by Cryo-Transmission Electron-Microscopy. Biophys J. 1989; 56:669–681. [PubMed: 2819233]
39. Cho HJ, et al. Measurement of ice thickness on vitreous ice embedded cryo-EM grids: investigation of optimizing condition for visualizing macromolecules. J Anal Sci Technol. 2013; 4:7.
40. Ludtke SJ, Chiu W. Focal pair merging for contrast enhancement of single particles. J Struct Biol. 2003; 144:73–78. [PubMed: 14643210]
41. Kaler EW, Murthy AK, Rodriguez BE, Zasadzinski JA. Spontaneous vesicle formation in aqueous mixtures of single-tailed surfactants. Science. 1989; 245:1371–1374. [PubMed: 2781283]
42. Li W, Huang Z, MacKay JA, Grube S, Szoka FC Jr. Low-pH-sensitive poly(ethylene glycol) (PEG)-stabilized plasmid nanolipoparticles: effects of PEG chain length, lipid composition and assembly conditions on gene delivery. J Gene Med. 2005; 7:67–79. [PubMed: 15515149]
43. Li W, Szoka FC Jr. Lipid-based nanoparticles for nucleic acid delivery. Pharm Res. 2007; 24:438–449. [PubMed: 17252188]
44. Ollivon M, Lesieur S, Grabielle-Madelmont C, Paternostre M. Vesicle reconstitution from lipid-detergent mixed micelles. Biochim Biophys Acta. 2000; 1508:34–50. [PubMed: 11090817]
45. Stuart MC, Boekema EJ. Two distinct mechanisms of vesicle-to-micelle and micelle-to-vesicle transition are mediated by the packing parameter of phospholipid-detergent systems. Biochim Biophys Acta. 2007; 1768:2681–2689. [PubMed: 17714686]
46. Mimms LT, Zampighi G, Nozaki Y, Tanford C, Reynolds JA. Phospholipid vesicle formation and transmembrane protein incorporation using octyl glucoside. Biochemistry. 1981; 20:833–840. [PubMed: 7213617]
47. Zumbuehl O, Weder HG. Liposomes of controllable size in the range of 40 to 180 nm by defined dialysis of lipid/detergent mixed micelles. Biochim Biophys Acta. 1981; 640:252–262. [PubMed: 7194112]
48. Philippot J, Mutaftschiev S, Liautard JP. A very mild method allowing the encapsulation of very high amounts of macromolecules into very large (1000 nm) unilamellar liposomes. Biochim Biophys Acta. 1983; 734:137–143.
49. Iinuma R, et al. Polyhedra self-assembled from DNA tripods and characterized with 3D DNA-PAINT. Science. 2014; 344:65–69. [PubMed: 24625926]
50. Gerling T, Wagenbauer KF, Neuner AM, Dietz H. Dynamic DNA devices and assemblies formed by shape-complementary, non-base pairing 3D components. Science. 2015; 347:1446–1452. [PubMed: 25814577]

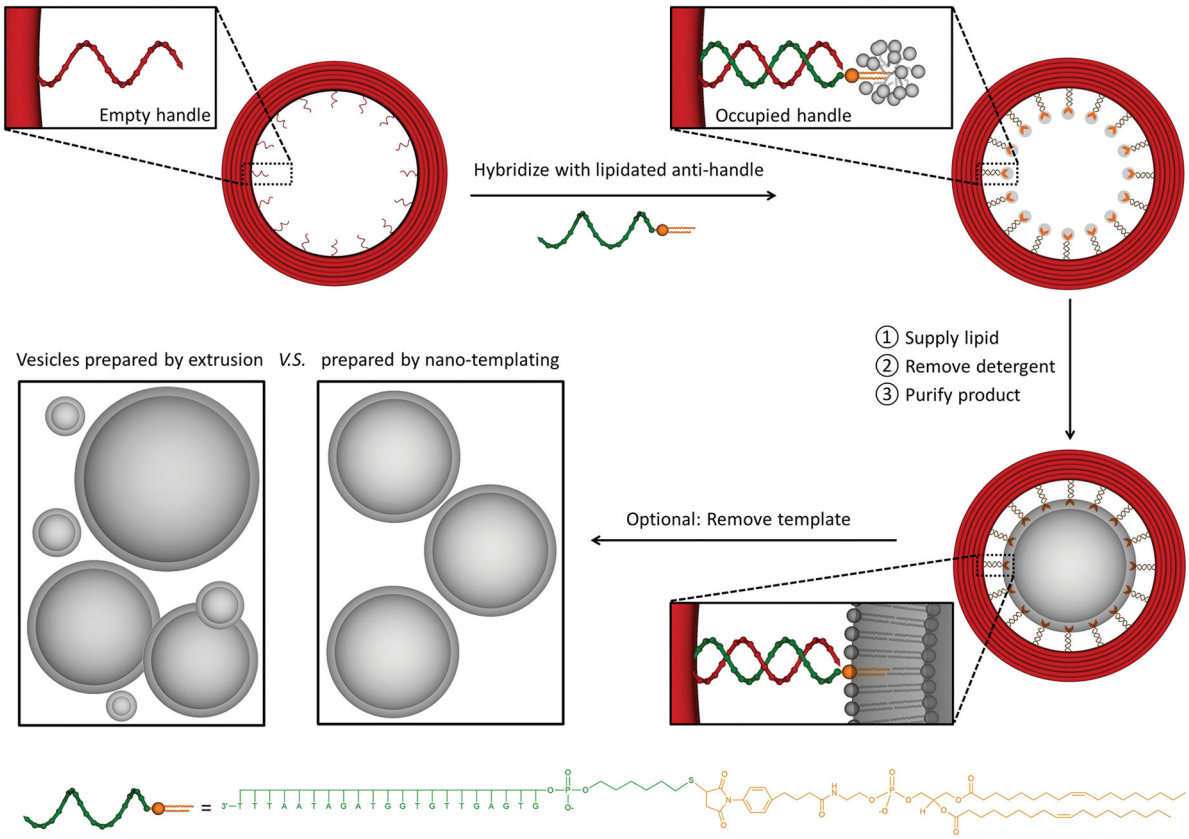

Figure 1.

Scheme of generating size-controlled vesicles by nano-templating. First, a DNA-origami ring (red) carrying multiple single-stranded extensions (empty handles) is constructed. Second, DNA anti-handles (oligonucleotides with complementary sequence to handles) are chemically conjugated to DOPE and incubated with the DNA ring to allow hybridization. Chemical structure of the lipidated anti-handle (green curl with orange arrowhead) is shown at the bottom of the figure. Third, the ring with occupied handles is mixed with extra lipid and detergent and dialyzed to allow vesicle formation. Desired product (liposomes with their size determined by the DNA template) is purified *via* isopycnic centrifugation. Finally, the vesicles (grey bubbles) can be released from the DNA ring, giving rise to a pool of liposomes with better homogeneity than those prepared by traditional methods such as extrusion.

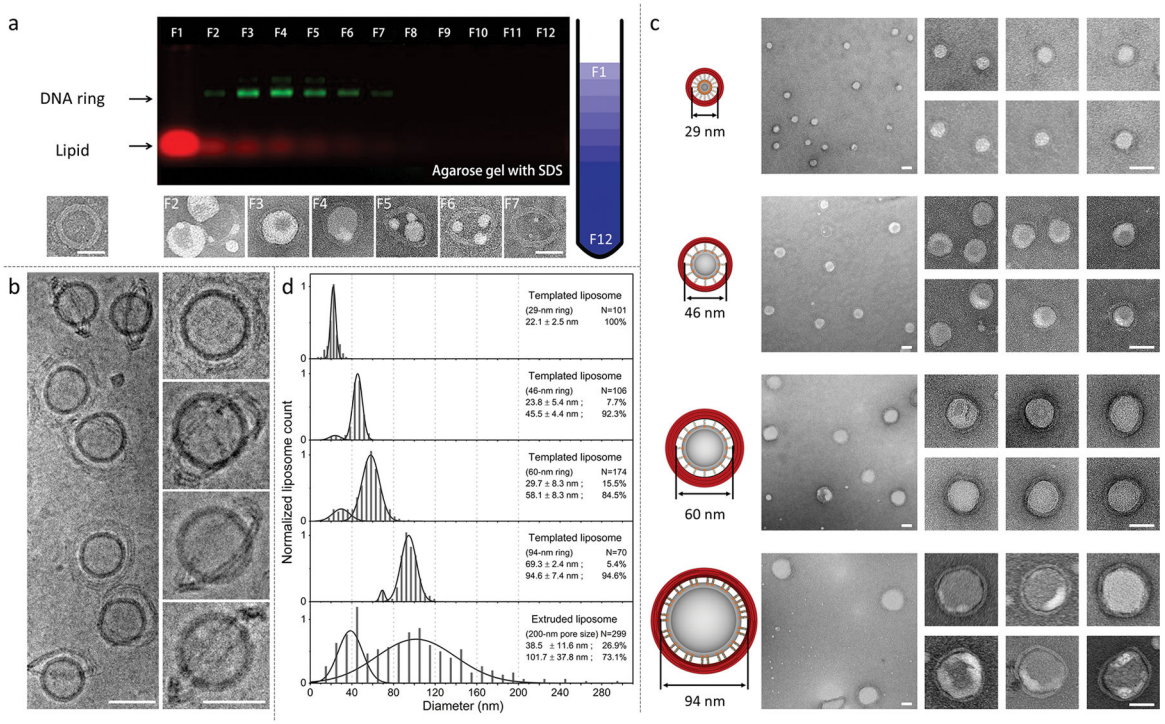

Figure 2.

Characterization of DNA templated liposomes. (a) The general workflow: resolving the density gradient fractions by agarose gel electrophoresis and imaging the fractions with TEM. Fractions are numbered sequentially from F1 to F12 from the top to the bottom of the gradient. A typical gel image is shown along with representative TEM images of fractions 2–7. A lipid-free 60-nm DNA ring is also shown for comparison. Note that the Cy5-labeled DNA ring and Rhodamine(B)-labeled lipid ran as two separate bands due to the presence of SDS during electrophoresis. (b) Cryo-EM images of liposomes formed inside 60-nm DNA rings after purification. (c) Representative TEM images of liposomes formed inside 29-, 46-, 60- and 94-nm DNA rings after purification. For each ring size, a cartoon model is shown on the left with corresponding TEM images shown on the right. Note that the cartoon models are drawn to scale with respect to one another. (d) Size distribution of templated *vs* extruded liposomes measured from negative-stain TEM images. Histograms of five liposome species are normalized to the same scale and fitted to Gaussian distribution curves. Fitting results (mean±std, weight) and sample size (N) are noted in the insets. Scale bars: 50 nm.

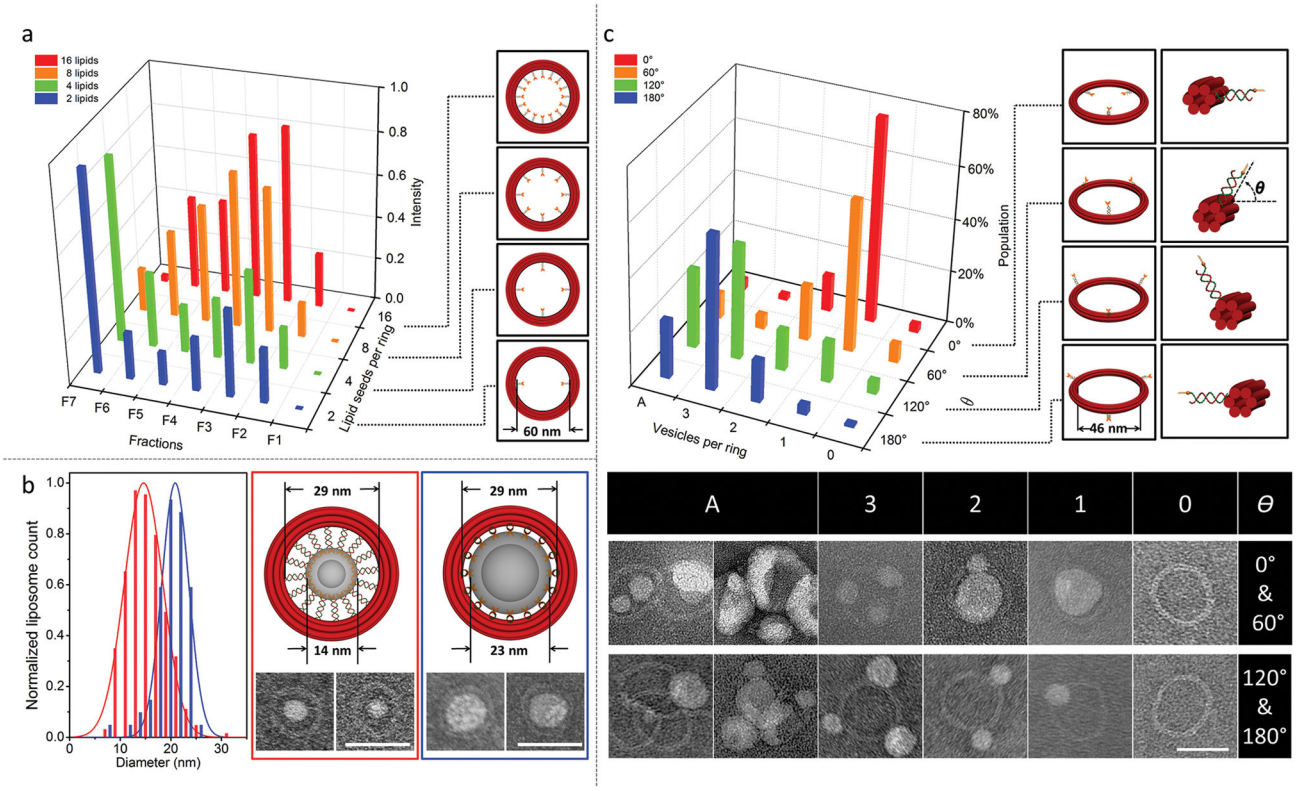

Figure 3.

Effect of initial lipid seed placement on final vesicle formation. (a) The lipid-seed number inside a 60-nm ring versus the yield of size controlled liposomes. The 3D bar graph is plotted based on the amount of DNA in each post-centrifugation fraction as measured by the DNA band intensity after gel electrophoresis. Fractions 3 and 4 (F3 and F4) contain liposomes with a designated size. Cartoon models of the four DNA ring constructs are shown on the right of the bar graph. (b) A comparison between two 29-nm rings with lipid seeds placed at different distances away from the inner edge of the ring. Representative TEM images and size distribution histograms are taken from the fraction that contains the most DNA rings. (c) Vesicles assembled on 46-nm rings with lipid seeds inside or outside of the ring. The assembly products are sorted into five categories based on the number of vesicles per ring (A= aggregates). Representative TEM images of each category are shown in a table and the occurrences of all types of product are plotted as a 3D bar graph. Data are taken from the same fraction for all four ring species. Scale bars: 50 nm.

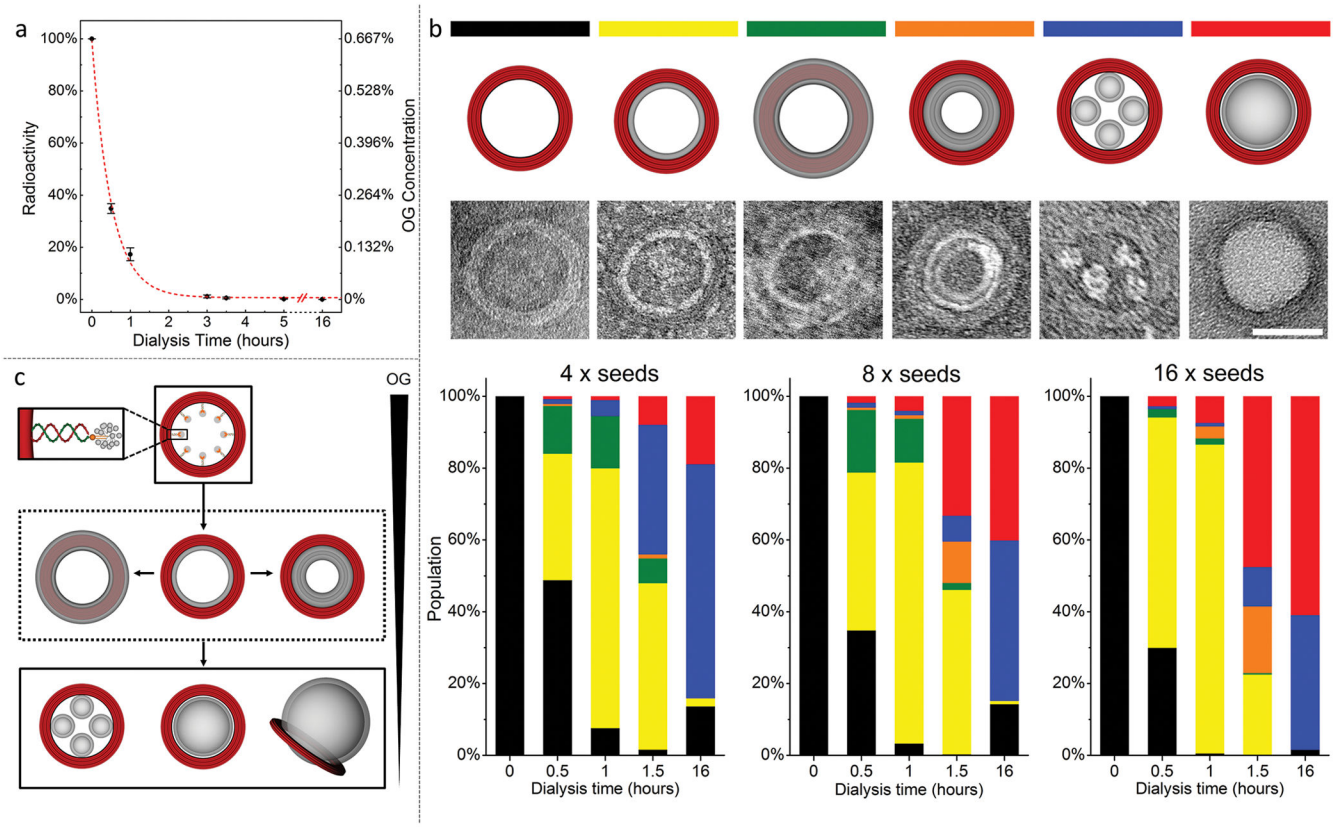

Figure 4.

Vesicle formation mechanism studied by capturing intermediates during dialysis. (a) Detergent removal monitored by the remaining radioactivity of ^{14}C-labeled OG at different time points. Error bars represent the standard deviations of 2–4 measurements. Dotted line is a fit using a single-exponential decay curve. (b) Top: A table summarizing the intermediates and final products. Cartoon models (lipid seeds are not drawn for clarity) and their color codes used in the bar graphs are shown on top of the corresponding TEM images. Scale bars: 50 nm. Bottom: Bar graphs illustrating a quantitative measure of all structures found at different time points (0, 0.5, 1, 1.5 and 16 hour) during the dialysis of rings with 4, 8 and 16 lipid seeds inside, 273≥N≥85. (c) A schematic diagram illustrating the hypothesized mechanism of the size-controlled liposome formation templated by a DNA ring. Cartoon models of starting material, intermediates and final products are shown in the top, middle and bottom rows, respectively.

Table 1

Buoyant density of the vesicles (60-nm ring template) affected by the lipid composition. Acronyms: DOPC = 1,2-dioleoyl-sn-glycero-3-phosphocholine, DPPC = 1,2-dipalmitoyl-sn-glycero-3-phosphocholine, Rhod-PE = 1,2-dioleoyl-sn-glycero-3-phosphoethanolamine-N-(lissamine rhodamine B sulfonyl) (ammonium salt), DOPS = 1,2-dioleoyl-sn-glycero-3-phospho-L-serine (sodium salt), DOTAP = 1,2-dioleoyl-3-trimethylammonium-propane (chloride salt).

Composition	DOPC	DPPC	Cholesterol	Rhod-PE	PEG-2k-PE	DOPS	DOTAP	Main product in[a,b]
0	79.2%	N/A	N/A	0.8%	5%	15%	N/A	Fractions 3 and 4
1	84.2%	N/A	N/A	0.8%	N/A	15%	N/A	Fractions 2 and 3
2	99.2%	N/A	N/A	0.8%	N/A	N/A	N/A	Fractions 2 and 3
3	89.2%	N/A	N/A	0.8%	N/A	N/A	10%	Fractions 1 and 2
4	N/A	49.2%	30%	0.8%	5%	15%	N/A	Fractions 3 and 4

[a] Fractions are numbered 1–12 from top to bottom of the density gradient (lightest fraction on top).

[b] DNA ring to lipid ratio ≈ 1:188,000